Cryogenics 81 (2017) 107–114

Contents lists available at ScienceDirect

Cryogenics

journal homepage: www.elsevier.com/locate/cryogenics

Research paper

Numerical modeling of critical-state magnetization in type-II superconducting cylinders under parallel and transverse magnetic field

S. Farinon [a], G. Iannone [b,*], P. Fabbricatore [a], U. Gambardella [b]

[a] INFN-Sezione di Genova, Via Dodecaneso, 33, 16146 Genova, Italy
[b] INFN-Sezione di Napoli, Via Cintia, 80126 Napoli, Italy

ARTICLE INFO

Article history:
Received 15 March 2016
Received in revised form 3 October 2016
Accepted 1 November 2016
Available online 2 November 2016

Index Terms:
Critical state
Finite element analysis
Hysteresis losses
Magnetization loop

ABSTRACT

In this paper we extensively analyze the magnetization of superconducting bulk cylinders in parallel and transverse magnetic field. We use analytic formulations with different $J_c(B)$ dependencies, and compare the magnetization to 2D and 3D numerical computations for finite geometries with different aspect ratios. This subject is a basic study for understanding the hysteretic losses in a cylindrical geometry, which is the typical geometry occurring in superconducting wires and cables. The shift of the peak of the magnetization cycle is always reproduced by FEM 2D and 3D, as a consequence of considering the local field in the $J_c(B)$. Using different $J_c(B)$ dependencies and different cylinder aspect ratio, we have reproduced the behavior of the magnetization in parallel fields, checking simulation results versus analytical calculations. In this framework we also developed the analytic behavior of the magnetization in parallel fields using the generalized Kim model. Finally, for a cylinder in a perpendicular magnetic configuration, we found that 2D numerical simulations, once suitably scaled, are in agreement to 3D simulations.

1. Introduction

Type II superconducting materials show magnetic irreversibility features leading to low temperature dissipations [1,2]. These hysteretic losses are crucial in the design of superconducting devices, thus the precise computation of the current density and the magnetic field distribution inside a conductor induced by an external magnetic field, or resulting from transport currents, is a common need.

In this context the use of numerical analyses based on Maxwell equations is mainly performed in the framework of the Bean's critical state model [3,4]. Within this framework, the computation by means of analytical expressions is usually either limited to simple geometries or to limited descriptions of the material's properties. For general shapes, analytical expressions can be hardly found, so numerical methods are to be preferred.

Finite Element Method (FEM) is a powerful tool to compute field profiles and current distributions inside a superconductor, thus it allows to evaluate the superconducting hysteresis losses.

Four major numerical approaches, featuring different equations, have been developed so far: the *A–V* formulation, based on the magnetic vector potential [5]; the *T–Ω* formulation, based on the current vector potential [6]; the *H*-formulation, based on the magnetic field [7–9]; and the Adaptive Resistive Algorithm (ARA) [10–12]. Further to FEM also calculation based on Variational Principles have been shown to be very powerful in several situations [13–16].

In order to perform a simulation able to reproduce the experimental behavior of Type II superconductors, the critical current density J_c, and its dependence on the internal magnetic field, is one of the key parameters that have to be taken into account. In general, the $J_c(B)$ dependence could be obtained either by electrical transport or magnetization measurements. In the electrical measurement the currents circulating through the sample generate a magnetic field that modifies the applied field in an inhomogeneous way. In the magnetic measurements, J_c is extracted from magnetic moment $m(B_a)$ of isothermal magnetization loops, where B_a is the external applied field, as:

$$J_c(B) = k \cdot \Delta M(B) \tag{1}$$

where k is a parameter depending on the sample geometry and ΔM is the width of the magnetization hysteresis loop, *i.e.* the magnetic moment per unit volume. For a cylinder of radius R with magnetic field parallel to its axis, we have $k = 3/(2R)$.

* Corresponding author at: INFN-Sezione di Napoli, Via Cintia, 80126 Napoli, Italy.
E-mail address: iannone@sa.infn.it (G. Iannone).

http://dx.doi.org/10.1016/j.cryogenics.2016.11.001
0011-2275/

This relation follows from the critical-state model in the approximation of infinitely long samples and J_c independent of the magnetic field [4]. Unfortunately, in a real sample this approximation is often not fully satisfied. Then, what is obtained from the width of the loop is not the required intrinsic $J_c(|B|)$ function, but a different function, $J_c(|B_a|)$.

In previous papers [17,18], we numerically reproduced the magnetization loops of a real superconducting sample in thin strips, disks and spherical geometries using the $J_c(|B_a|)$ dependence by the means of the Adaptive Resistive Algorithm (ARA) approach and the H-formulation, and we found a full agreement between these two FEM approaches.

In this paper we extensively analyze the magnetization of a bulk superconductor having a cylindrical shape with radius R and a finite length L, when a varying magnetic field $B_a(t)$ is applied parallel or transverse to its axis. To better describe the features of the magnetization loop we use the local field value in the dependence of $J_c(|B|)$. 2D numerical simulations are based on the H-formulation, while 3D numerical simulations are performed using the ARA approach.

The numerical simulations were done using two different hardware: the H-formulation was implemented under the COMSOL® Multiphysics version 4.3 installed on a 2.3 GHz six core dual Intel Xeon E52630 Lenovo Thinkstation with 64 GB RAM; the ARA approach was implemented within ANSYS© version 16.2 installed on a 3.5 GHz two core Intel Xeon Processor E5-1650 v3 with 64 GB RAM [19].

The analysis, is carried out with two different aspect ratios $\beta = R/L$, *i.e.* $\beta = 2$ and $\beta = 10$. In Section 2 we first present the analytical expressions for the magnetization derived from the Bean, exponential, Kim, and generalized Kim dependence of $J_c(B)$ in parallel field. In particular, the analytical expressions for generalized Kim dependence of $J_c(B)$, is originally developed in this paper. The analytical solution for the magnetization in perpendicular field only exists for $J_c(B) =$ constant, *i.e.* the Bean model. In Section 3 we show how numerical 2D and 3D simulations compare to the analytical solutions, in the case of parallel field, for each considered $J_c(B)$ behavior. In the perpendicular field configuration we first compare numerical simulation to the only analytical case available, *i.e.* $J_c(B) =$ const., finding the scaling factor which allows to use faster 2D simulations to reproduce the 3D results. In these simulations, we use the local field in the $J_c(B)$ behavior and, consequently, we reproduce the actual shift of the peak of the magnetization in the $m(B)$ cycle. Then we compare the 3D and 2D simulation performed in the exponential and generalized Kim dependence of the $J_c(B)$, showing that the same scaling factor may be used in a 2D numerical computation to reproduce the 3D simulation result. In Section 4 the conclusions are drawn.

2. Analytic long cylinder in parallel and transverse magnetic field

The simplest way to describe a type-II superconductor subject to a varying magnetic field is the Bean critical state model [3,4]. This model assumes that the local magnetic field inside a sample is associated to a constant critical current density J_c by means of the Ampere's law: $\nabla \times \vec{B} = \mu_0 J_c$. In order to take into account the dependence of the J_c on the magnetic field, in the past years, several enhancements to the Bean critical state model have been proposed. In particular, we are going to investigate analytically the behavior of a long cylinder, R in radius and L in length, exposed to a varying magnetic field $B_a(t) = B_0 \sin(\omega t)$ with the following $J_c(B)$ dependence: the Bean model $J_c(B) = J_{c0}$, the exponential model $J_c(B) = J_{c0} e^{-B/B_0}$ [20], the Kim model $J_c(B) = J_{c0}/(1 + B/B_0)$, and the generalized Kim model $J_c(B) = J_{c0}/(1 + B/B_0)^\gamma$ [21].

2.1. Analytic long cylinder in parallel magnetic field

The analytic model for a long cylinder with magnetic field parallel to its axis has been solved by Brandt for the Bean model [4,22], Chen et al. [23,24], and by Johansen and Bratsberg [25] for the exponential and Kim models.

In the Bean model, the virgin magnetic moment is found to be:

$$m = \begin{cases} -\pi J_c R^3 L (b_a - b_a^2 - b_a^3/3) & 0 < b_a < 1 \\ -\pi J_c R^3 L/3 & b_a \geqslant 1 \end{cases} \tag{2}$$

where $b_a = B_a/B_p$ and $B_p = \mu_0 J_c R$ is the full penetration field. Reminding that $B_a = B_0 \sin\omega t$, the other branches of the magnetization curve can be found using the usual relations [22]:

$$m_\downarrow(B_a, B_0) = m(B_0) - 2m\left(\frac{B_0 - B_a}{2}\right) \tag{3}$$

$$m_\uparrow(B_a, B_0) = -m(B_0) + 2m\left(\frac{B_0 + B_a}{2}\right) \tag{4}$$

According to [25], the solution of the exponential model is given by:

$$\frac{\mu_0 M}{B_0} = \begin{cases} -b_a + \frac{2}{k}[1 - (1 - b_a)e^{b_a}] + \frac{1}{2k^2}[1 - 4e^{b_a} + (3 - 2b_a)e^{2b_a}] & 0 < b_a < b_p \quad \text{virgin increasing} \\ \left(1 - \frac{2}{k}e^{b_a} + \frac{1}{k^2}e^{2b_a}\right)\ln(1 - ke^{-b_a}) - \frac{3}{2} + \frac{1}{k}e^{b_a} & b_a \geqslant b_p \quad \text{virgin increasing} \\ \left(1 + \frac{2}{k}e^{b_a} + \frac{1}{k^2}e^{2b_a}\right)\ln(1 + ke^{-b_a}) - \frac{3}{2} - \frac{1}{k}e^{b_a} & b_a \geqslant 0 \quad \text{decreasing} \\ -\frac{1}{2k^2}[1 - 4e^{b_m} + (3 - 2b_m)e^{2b_m}] - \frac{2}{k}[1 - (1 + b_a)e^{-b_a}] & \\ \quad -\frac{1}{2k^2}[1 - 4e^{-b_a} + (3 + 2b_a)e^{-2b_a}] - b_a & -b_p < b_a < 0 \quad \text{decreasing} \\ -\left(1 - \frac{2}{k}e^{-b_a} + \frac{1}{k^2}e^{-2b_a}\right)\ln(1 - ke^{b_a}) + \frac{3}{2} - \frac{1}{k}e^{-b_a} & b_a \leqslant -b_p \quad \text{decreasing} \end{cases} \tag{5}$$

where $m = \pi R^2 L M$, $k = B_P/B_0$, $b_p = \ln(1 + k)$ and $b_m = \ln(2 + k - e^{-b_a})$.

Following the same calculation scheme proposed in [25], we also derived the solution for the generalized Kim model:

$$\frac{\mu_0 M}{B_0} = \begin{cases} F(b_a, b_m, k) & b_m = 0 & 0 < b_a < b_p & \text{virgin increasing} \\ F(b_a, b_m, k) & b_m = \sqrt[\gamma+1]{(1+b_a)^{\gamma+1} - (\gamma+1)k} - 1 & b_a \geqslant b_p & \text{virgin increasing} \\ F(b_a, b_m, -k) & b_m = \sqrt[\gamma+1]{(1+b_a)^{\gamma+1} + (\gamma+1)k} - 1 & b_a \geqslant 0 & \text{decreasing} \\ G(b_a, b_m, k) & b_m = \sqrt[\gamma+1]{2 - (1-b_a)^{\gamma+1} + (\gamma+1)k} - 1 & -b_p < b_a < 0 & \text{decreasing} \\ -F(-b_a, b_m, k) & b_m = \sqrt[\gamma+1]{(1-b_a)^{\gamma+1} - (\gamma+1)k} - 1 & b_a \leqslant -b_p & \text{decreasing} \end{cases} \tag{6}$$

where

$$\begin{aligned} F(b_a, b_m, k) = & -(b_a - b_m) + \frac{2}{(\gamma+1)k}(1+b_a)^{\gamma+1}(b_a - b_m) \\ & - \frac{2}{(\gamma+1)(\gamma+2)k}[(1+b_a)^{\gamma+2} - (1+b_m)^{\gamma+2}] \\ & - \frac{1}{(\gamma+1)^2 k^2}\Big[(1+b_a)^{2(\gamma+1)}(b_a - b_m) \\ & - \frac{2(1+b_a)^{\gamma+1}}{(\gamma+2)}((1+b_a)^{\gamma+2} - (1+b_m)^{\gamma+2}) \\ & + \frac{1}{(2\gamma+3)}((1+b_a)^{2\gamma+3} - (1+b_m)^{2\gamma+3})\Big] \end{aligned} \tag{7}$$

$$\begin{aligned} G(b_a, b_m, k) = & -b_a + \frac{2}{(\gamma+1)k} \times \left[\frac{1}{\gamma+2}(1-b_a)^{\gamma+2} + (1-b_a)^{\gamma+1} b_a - \frac{1}{\gamma+2}\right] \\ & + \frac{1}{(\gamma+1)^2 k^2}\left[b_m(1+b_m)^{2\gamma+2} - \frac{3\gamma+4}{(\gamma+2)(2\gamma+3)}(1+b_m)^{2\gamma+3} \right. \\ & \left. + \frac{2(1+b_m)^{\gamma+1}}{(\gamma+2)} - \frac{1}{(2\gamma+3)}\right] \\ & - \frac{1}{(\gamma+1)^2 k^2}\left[b_a(1-b_a)^{2\gamma+2} + \frac{3\gamma+4}{(\gamma+2)(2\gamma+3)}(1-b_a)^{2\gamma+3} \right. \\ & \left. - \frac{2(1-b_a)^{\gamma+1}}{(\gamma+2)} + \frac{1}{(2\gamma+3)}\right] \end{aligned} \tag{8}$$

and

$$m = \pi R^2 L M, \quad k = \mu_0 J_{c0} R / B_0, b_p = \sqrt[\gamma+1]{1 + (\gamma+1)k} - 1.$$

In all the previous cases, it is possible to demonstrate that the saturated magnetic moment ($b_a \gg b_p$) is given by $m_{sat} = -\pi J_c(B) R^3 L/3$, where $J_c(B)$ is the critical current density as function of the magnetic field for the considered model.

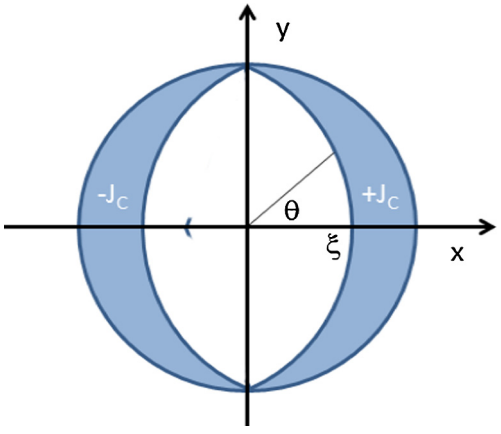

Fig. 1. Cross section view of the cylinder showing the current penetration front.

2.2. Analytic long cylinder in transverse magnetic field

The solution of the problem of a long cylinder subject to a transverse magnetic field perpendicular to the cylinder axis, is usually found through an approximated approach to the Bean critical state model. The inner boundary of the shielding currents is aprioristically assumed to be an ellipse whose ellipticity follows the varying field. In this framework, an interesting solution has been proposed by Gömöry et al. [26] for a superconducting strip with an elliptic cross section in a perpendicular magnetic field. In the cylinder case, the current carrying region extends up to a boundary which can be described by a one-parameter family of closed curves given by:

$$u = \sqrt{x^2 + y^2} = \frac{R\xi}{\sqrt{1 - (1 - \xi^{2-2/n})\sin^2\theta}} \tag{9}$$

where n is a parameter, θ is the polar angle, and ξ represents the position of the front on the x axis as illustrated in Fig. 1. This corresponds to the assumption that flux fronts are ellipses with semi-axis $R\xi$ e $R\xi^{1/n}$. The solution to the same problem found by Bhagwat and Chaddah in [27] is included in this description and corresponds to $n = 2$.

The magnetic moment can be calculated as:

$$\begin{aligned} m(\xi) &= -L\int_{S_{J_c}} x J_c dS = -4 J_c L \int_0^{\pi/2}\int_u^R r^2 \cos\theta dr d\theta \\ &= -\frac{4}{3} J_c L \int_0^{\pi/2} \cos\theta \left[R^3 - \left(\frac{R\xi}{\sqrt{1 - (1 - \xi^{2-2/n})\sin^2\theta}}\right)^3\right] d\theta \\ &= -\frac{4}{3} J_c R^3 L (1 - \xi^{2+1/n}) \end{aligned} \tag{10}$$

where S_{J_c} is the region of the screening currents. To calculate the strength of the external field needed to give rise to the flux front $u(\xi,\theta)$ we consider the property that the screening field must be exactly equal and opposite to the external field change, in order to achieve perfect screening of the interior. Since the field of the interior must be uniform, we may simply calculate it in the origin using the Biot-Savart law:

$$\begin{aligned} B(\xi) &= -\int_{S_{J_c}} \left(\frac{\mu_0 J_c}{2\pi r}\right)\cos\theta dr d\theta = -4\frac{\mu_0 J_c}{2\pi}\int_0^{\pi/2}\int_u^R \cos\theta dr d\theta \\ &= -\frac{2\mu_0 J_c}{\pi}\int_0^{\pi/2}\cos\theta\left[R - \frac{R\xi}{\sqrt{1 - (1 - \xi^{2-2/n})\sin^2\theta}}\right] d\theta \\ &= -\frac{2}{\pi}\mu_0 J_c R\left(1 - \xi\frac{\arcsin\sqrt{1 - \xi^{2-2/n}}}{\sqrt{1 - \xi^{2-2/n}}}\right) \end{aligned} \tag{11}$$

As expected, the full penetration field, corresponding to $\xi = 0$, is given by $B_p = \frac{2}{\pi}\mu_0 J_c R$.

The saturated magnetic moment for an infinitely long cylinder can be deduced from Eq. (10) at $\xi = 0$ and is given by

$m_{sat} = -4J_cR^3L/3$. In [26] it is suggested that optimum value for n exponent, at least at low field, can be found by imposing [28]:

$$\chi_0 = \lim_{\xi\to 1}\chi_a = \lim_{\xi\to 1}\frac{M(\xi)}{B(\xi)} = 2 \tag{12}$$

where χ_0 is the susceptibility in the Meissner state, χ_a is the amplitude susceptibility and

$$M(\xi) = \frac{\mu_0 m(\xi)}{\pi R^2 L} = -\frac{4}{3\pi}J_cR(1-\xi^{2+1/n}) \tag{13}$$

Unfortunately the limit in Eq. (12) results to be 2 regardless of the value of the n exponent. A possible way round, is to impose the value for χ_0 in the more general case of an elliptic strip (with semi-axis a and b) of aspect ratio $\Gamma = b/a$:

$$\chi_0 = \lim_{\xi\to 1}\frac{M(\xi)}{B(\xi)} = \frac{2}{3}\frac{(1-\xi^{2+1/n})}{\frac{\arcsin\sqrt{1-\frac{1}{\Gamma^2}}}{\sqrt{1-\frac{1}{\Gamma^2}}} - \xi\frac{\arcsin\sqrt{1-\frac{\xi^{2-2/n}}{\Gamma^2}}}{\sqrt{1-\frac{\xi^{2-2/n}}{\Gamma^2}}}} = 1+\frac{1}{\Gamma}, \tag{14}$$

Then, it is possible to obtain the n value from the previous equation:

$$n(\Gamma) = \frac{2\Gamma - 5 + 3k}{1 - 4\Gamma + 3\Gamma^2 k}, \quad k = \frac{\operatorname{arcsinh}\sqrt{\frac{1-\Gamma^2}{\Gamma}}}{\sqrt{1-\Gamma^2}}, \tag{15}$$

and finally get the limit for a cylinder as

$$n_{opt} = \lim_{\beta\to 1} n(\Gamma) = \frac{7}{2} \tag{16}$$

In order to compare the results coming from the 2D model to the 3D models, we are looking for a correction factor which allows the calculation of the magnetic moment for a finite long cylinder just by performing 2D simulation, as occurred for the superconducting strip geometry [17]. We can start from the logic assumption that the currents have, on each section normal to the y axis, a strip-like behavior as shown in Fig. 2.

As shown in Fig. 3, this behavior is not perfectly followed, *i.e.* currents do not turn at fixed $\alpha = 45°$ on each cutting plane by varying h. We found the opposite: currents turn at constant h by varying α. The longitudinal location where the current starts turning, h, has to be found.

On each section of the cylinder we have a different angle α given by the relation $h = L/2 - a/\tan\alpha$, and on each infinitesimal layer with thickness dy, the corresponding infinitesimal saturated magnetic moment is given by:

$$dm_{sat} = 4\cdot\frac{1}{2}\cdot J_c\cdot dy\left(-\int_0^a x dx\int_0^{h+\frac{x}{a}(\frac{L}{2}-h)} dz + \int_h^{L/2} z dz\int_{\frac{z-h}{\frac{L}{2}-h}a}^0 dx\right)$$
$$= -\frac{1}{12}J_c a dy(L^2 + 2La - Lh + 2ah - 2h^2) \tag{17}$$

The total saturated magnetic moment can be obtained by replacing $a = R\cos\theta$, $y = R\sin\theta$, $dy = R\cos\theta d\theta$ and integrating, where θ is the angle in polar coordinates:

$$\mathrm{m_{sat}} = -2\cdot\frac{1}{12}\cdot \mathrm{J_c}\cdot\int_0^{\pi/2} \mathrm{R^2\cos^2\theta(L^2 + 2LR\cos\theta - Lh} + 2\mathrm{hR}\cos\theta - 2\mathrm{h^2})d\theta$$
$$= -\frac{4}{3}\mathrm{J_cR^3L}\cdot\left(\frac{9\pi\mathrm{LX} - 6\pi\mathrm{X^2} + 24\mathrm{LR} - 16\mathrm{RX}}{48\mathrm{RL}}\right) \tag{18}$$

where we made the replacement $h = L/2 - X$. To get the value of x we impose that $\lim_{L\to\infty} m_{sat} == -\frac{4}{3}J_cR^3L$, so that:

$$\frac{3\pi\mathrm{X} + 8\mathrm{R}}{16\mathrm{R}} = 1, \quad \mathrm{X} = \frac{8\mathrm{R}}{3\pi} \tag{19}$$

which corresponds on the mid plane to an angle of current turn $\alpha = \tan^{-1}\frac{\mathrm{R}}{\mathrm{X}} = \tan^{-1}\frac{3\pi}{8} = 49.7°$.

The saturated moment is then finally given by:

$$\mathrm{m_{sat}} = -\frac{4}{3}\mathrm{J_cR^3L}\left[1 - \frac{16}{9\pi}\frac{\mathrm{R}}{\mathrm{L}}\right] \tag{20}$$

It may be worth noting that same calculation, in the thin strip case (width a, thickness d and length L), lead to $\alpha = 45°$ as reported in [17].

In conclusion, for a cylinder in the transverse magnetic field, we can assume $m_{sat} = m_{sat[L=\infty]} * \eta$ where the coefficient:

$$\eta = 1 - \frac{16}{9\pi}\frac{\mathrm{R}}{\mathrm{L}} \tag{21}$$

represents the correction which must be applied to the moment computed for an infinitely long cylinder when dealing with a finite length cylinder. In the next section we shall use this η for the Kim and exponential model of the cylinder in transverse magnetic field, where, to our knowledge, it does not yet exists any analytical expression for the magnetization.

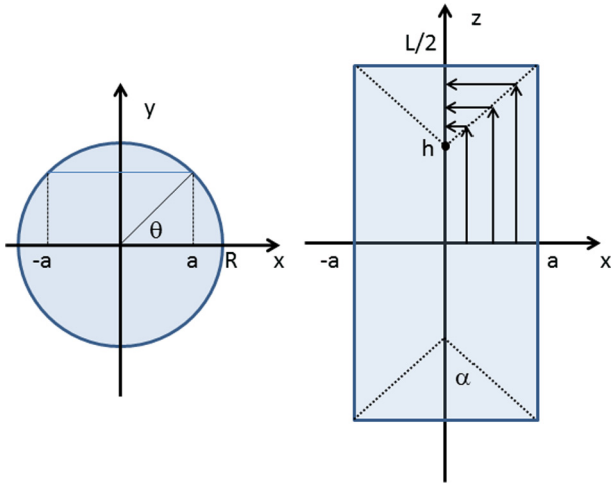

Fig. 2. Cut planes perpendicular (left) and parallel (right) to the cylinder axis where the screening currents circulates.

3. Results and discussion

In order to compare our simulations against the analytical results, reported in Section 2, we choose to study two different cylindrical shapes. The first one is a cylinder with $L = 10$ mm and $R = 1$ mm, while the second one is a cylinder with $L = 2$ mm and $R = 1$ mm. We decided to choose this two aspect ratios in order to explore the differences in the magnetization loops against $\beta = L/R$. In all the numerical simulations the J_{c0} value is fixed to $5\cdot 10^8$ A/m^2, and the γ exponent in the generalized Kim model is fixed to $\gamma = 4$.

The 2D FEM analyses are carried out in the axisymmetric mode. The cylinder is meshed with 400 elements and the analysis lasts about 2 h. The 3D analyses are carried out in 1/8 symmetry. The cylinder is meshed with about 5000 elements and the analyses require about 20 h computation.

3.1. Magnetic field parallel to the cylinder axis

In Fig. 4a are shown the curves computed in the Bean model, by using Eqs. (2)–(4), and the corresponding 2D numerical computa-

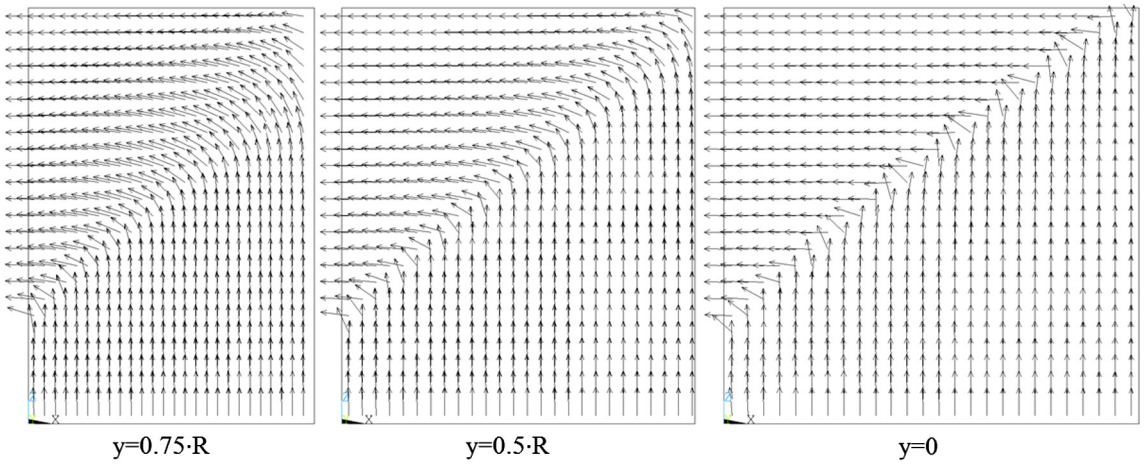

Fig. 3. 3D FEM current paths in the *x-z* planes at different *y* (i.e. field direction) in 1/4 symmetry (I quadrant shown on right part of Fig. 2) for a cylinder with $L = 2R$ under $B = 1\text{T}$ and $J_c = 5 \cdot 10^8\ \text{A/m}^2$.

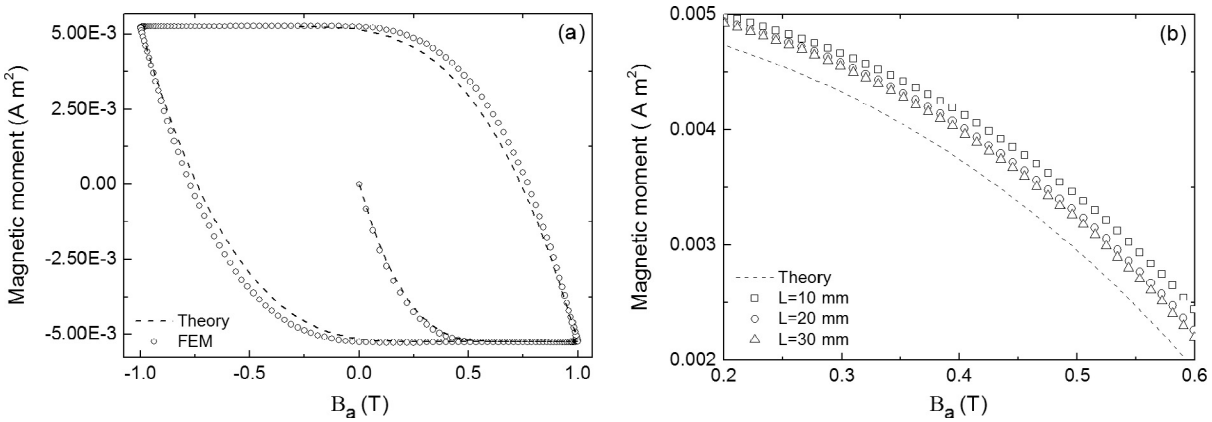

Fig. 4. Plot of Eqs. (2)–(4) compared to 2D FEM simulation: (a) whole cycle with L = 10; (b) enhanced region showing the effect of increasing L in the 2D FEM.

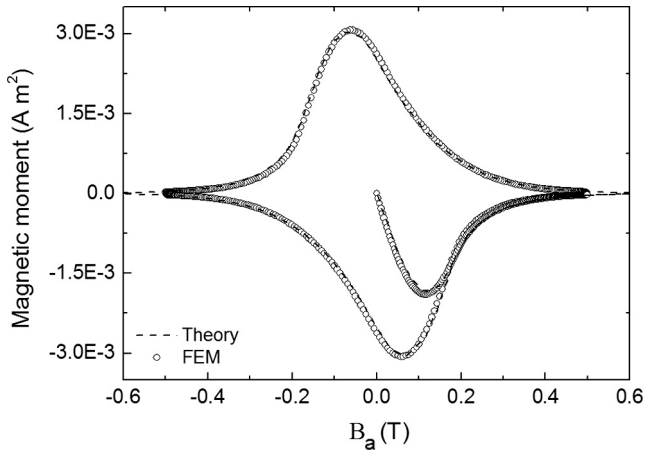

Fig. 5. Analytical and numerical plots of the magnetic moment in parallel field for a cylinder with β = 10 assuming an Exponential dependence in J_c(B). The analytical solution follow from Eq. (5).

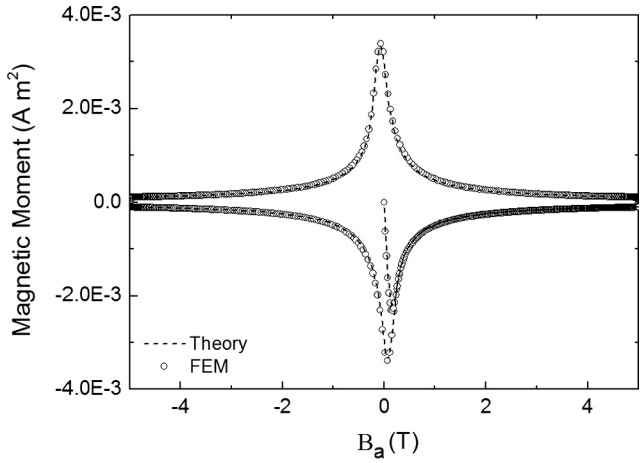

Fig. 6. Analytical and numerical plots of the magnetic moment in parallel field for a cylinder with β = 10 assuming a Kim dependence in J_c(B). The analytical solution follow from Eq. (6) with γ = 1.

tion performed using the *H*-formulation. The difference arises from the fact that the analytical solution reported in [22] is developed for an infinitely long cylinder, *i.e.* $\beta \to \infty$. This feature is more explicitly summarized in Fig. 4b), where it is shown how the increment of β moves the FEM curves towards the analytical one.

Considering the $J_c(B)$ exponential dependence, we show the comparison between the analytical solution derived from Eq. (5), and the FEM simulation in Fig. 5. It is useful to note that using the local field for $J_c(B)$, the agreement is complete both in the virgin magnetization state and in the whole magnetization cycle,

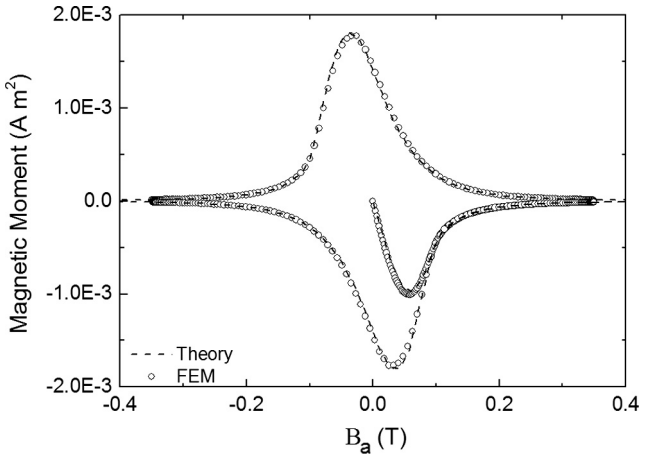

Fig. 7. Analytical and numerical plots of the magnetic moment in parallel field for a cylinder with β = 10 assuming a generalized Kim dependence in $J_c(B)$. The analytical solution follow from Eq. (6) with γ = 4.

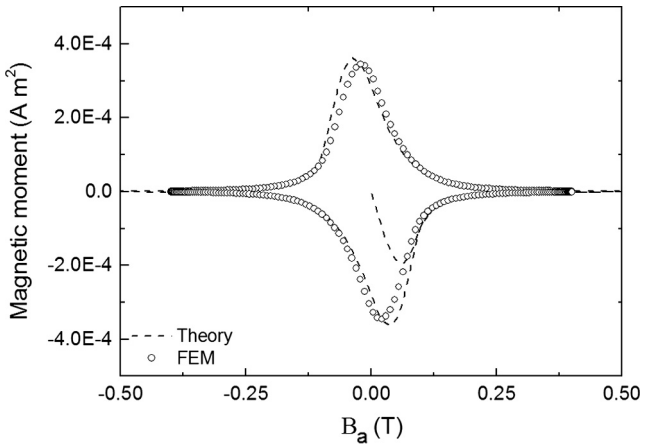

Fig. 8. Analytical and numerical plots of the magnetic moment in parallel field for a cylinder with β = 2 and 10 assuming a generalized Kim model with γ = 4 for $J_c(B)$.

including the peak positions of the magnetization cycles. In Figs. 6 and 7 we show the plot of the analytical solution derived from Eq. (6), and the corresponding FEM simulations in the case of both Kim model, and generalized Kim model, respectively.

Again the agreement is more than satisfactory using these two $J_c(B)$ dependencies. Thus we could conclude that the 2D FEM numerical simulations are able to compute the magnetization cycles, and hence the losses associated with the considered model. In these specific cases we only used *H*-formulation, but we already demonstrated the full agreement between ARA approach and *H*-formulation [17,18].

In order to investigate the effect of decreasing β in this parallel configuration, we also analyzed the behavior of the magnetization peak position on the applied magnetic field. In Fig. 8 we show the magnetization cycle in the framework of the generalized Kim model with $\gamma = 4$ and $\beta = 2$. In this case there is a partial agreement between the analytical and FEM curves. Again this effect can be ascribed to the finite nature of the sample respect to the infinite sample considered in the theory.

This feature has been also studied by Sanchez and Navau [29] by using a different approach. In our computation changing the β values, we found the same behavior of the magnetization peak observed in [29], *i.e.* the magnetization peak moves towards negative *x*-axis as the β grows.

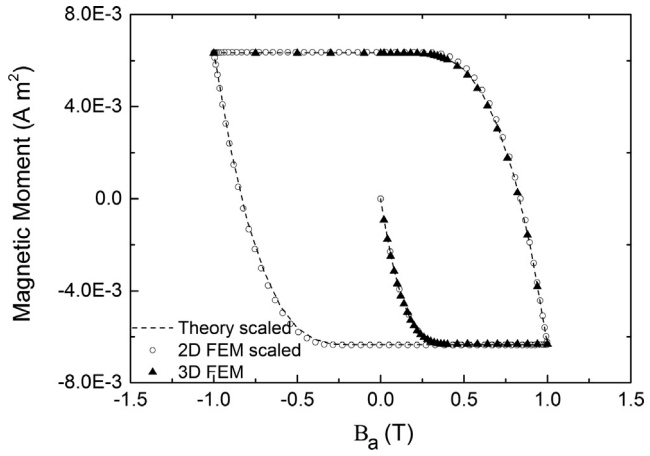

Fig. 9. Analytical and numerical plots of the magnetic moment in perpendicular field for a cylinder with β = 10 assuming a Bean model for $J_c(B)$. Both theory and 2D simulation are scaled with the same factor η = 0.943.

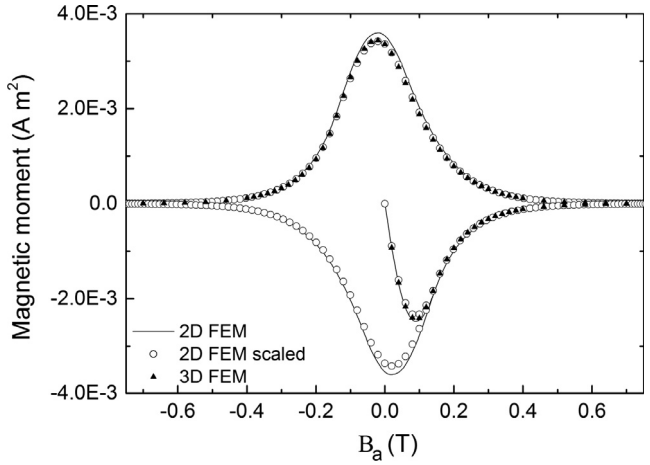

Fig. 10. Numerical plots of the magnetic moment in perpendicular field for a cylinder with β = 10 assuming a exponential dependence in $J_c(B)$.

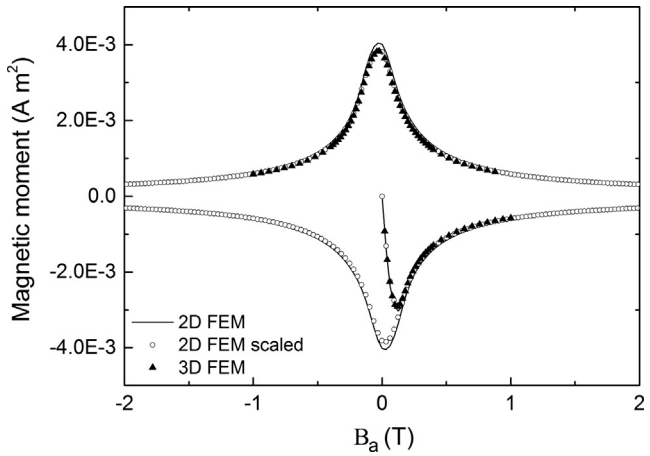

Fig. 11. Numerical plots of the magnetic moment in perpendicular field for a cylinder with β = 10 assuming a Kim dependence in $J_c(B)$.

3.2. Magnetic field perpendicular to the cylinder axis

When the magnetic field is perpendicular to the cylinder axis, the axial symmetry is lost. In this case we expect that the finite

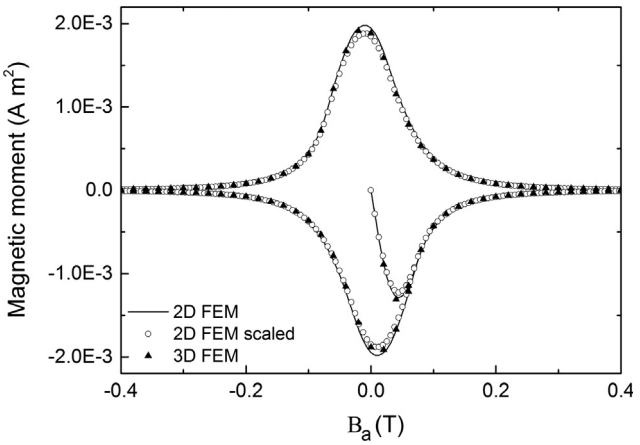

Fig. 12. Numerical plots of the magnetic moment in perpendicular field for a cylinder with β = 10 assuming a generalized Kim dependence, γ = 4, in J_c(B).

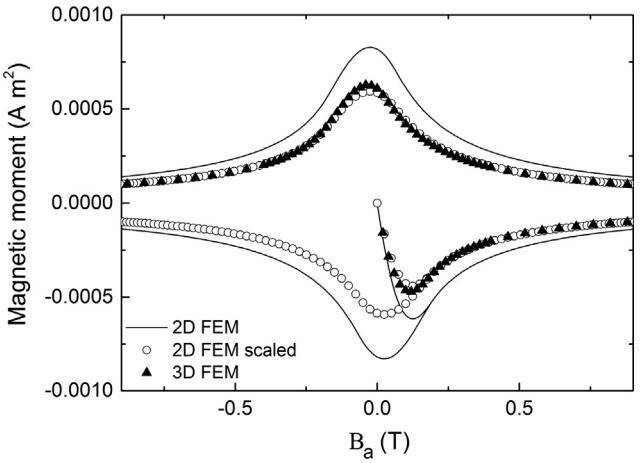

Fig. 14. Numerical plots of the magnetic moment in perpendicular field for a cylinder with β = 2 assuming a Kim dependence in J_c(B).

length L plays a more important role in determining the shape of the magnetization cycles. In this case the analytical solutions are available just only for the Bean model [30] thus, our first step was to make a comparison between this analytical solution and the 2D simulation, both referred to an infinite long cylinder. This comparison gives a perfect matching.

Dealing with 3D simulation, we note that analytical results and 2D simulation have to be scaled with the η factor defined in Eq. (21), in order to match the 3D one. In fact η, defined in Eq. (21), actually keeps into account of the current closure in a sample having a finite length. The results obtained for the Bean model and $\beta = 10$ are summarized in Fig. 9. In this graph we report the analytical solution and the 2D simulation (both scaled with factor $\eta = 0.943$) together with the 3D simulation. It can be noted a good agreement among curves with a maximum deviation of about 2%.

Concerning the exponential decay model in the $J_c(B)$, where to our knowledge no analytical theory have be developed so far, we again find that 2D simulation, rescaled with the same factor $\eta = 0.943$, reproduces the 3D simulation. This result is shown in Fig. 10 where the 2D model provides a hysteretic cycle larger than the one computed in the 3D model. When we apply the scaling factor η to the 2D results we find again that the 2D scaled curve overlaps the 3D computed curve.

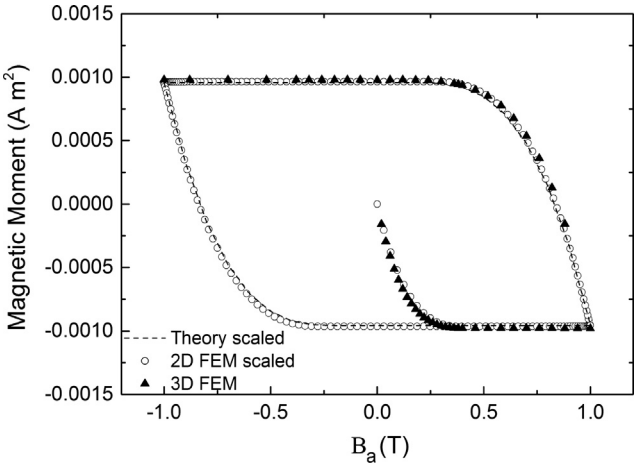

Fig. 13. Analytical and numerical plots of the magnetic moment in perpendicular field for a cylinder with β = 2 assuming a Bean model for J_c(B). Both theory and 2D simulation are scaled with the same factor η = 0.717.

The same occurrence is found in the Kim and generalized Kim models for $J_c(B)$, as shown in Figs. 11 and 12, respectively.

Being this occurrence evident for $\beta = 10$, we performed the same numerical approach for a $\beta = 2$ in order to verify how the β value affects the magnetization cycle even in this case. The result, shown in Fig. 13, has to be compared to Fig. 9. As expected, the moment scales with the superconducting volume, but the 2D numerical solution is notably different from the analytical solution or the 3D numerical simulation. Also in this case the correcting coefficient $\eta = 0.717$, is again effective to overlap the 2D FEM scaled curve to the correct 3D and analytical curves.

In this picture a small discrepancy (roughly 2%) is more evident among curves, then in Fig. 9. This occurrence may be ascribed to fact that in Eq. (20) only straight current paths are taken into account. This is just an approximation as shown in Fig. 3. Of course this is less evident in Fig. 9 because the magnetization became lower upon the raising of L/R ratio as written in Eq. (20). In Fig. 14 the same occurrence is shown, considering the Kim model and $\beta = 2$.

In conclusion we have found that in the perpendicular condition the 2D numerical approach can be suitably used to compute the magnetization cycle of a finite length cylinder. Even if the η factor has been derived analytically in the Bean model, we get evidence that it can be used generally in the framework of other critical state models. This approach saves computation time when compared to the 3D numerical integration.

4. Conclusion

In order to analyze the magnetization cycle of a bulk superconductor having a cylindrical shape, we examined the possible analytical solution of $m(B)$ for the magnetic field applied in parallel and perpendicular configurations, using the local field in the $J_c(B)$ behavior.

Different critical state models are considered: Bean, exponential, Kim, and generalized Kim with $\gamma = 4$. Concerning the latter model, we also developed the $m(B)$ analytical expression in the parallel configuration. We then compared the available analytical expression to 2D and 3D numerical simulations, performed for two different cylinder aspect ratios: $L/R = 10$ and $L/R = 2$. The simulations compute the magnetic moment taking into account of the local field for each of the $J_c(B)$ model, and an excellent agreement is found among analytic expressions and numerical simulations both in parallel and in perpendicular field configuration. In particular, in the latter configuration we find, from the analyses using the Bean

model, a numerical factor that can be used to suitably scale the fast 2D computation, and reproduce the 3D simulation. We also demonstrated that the same factor can be used to scale 2D simulation also in all the other critical state models investigated.

Acknowledgment

Authors are grateful to A. Saggese for fruitful discussion.

References

[1] Poole Jr CP, Farach HA, Creswick RJ, Prozorov P. Superconductivity. Academic Press; 2010.
[2] Iannone G, Quero F, Gambardella U, Fabbricatore P, Farinon S, Volpini G. Composite superconducting wires for fast ramped magnets. Composites Part B 2016;90:133–40.
[3] Bean CP. Magnetization of hard superconductors. Phys Rev Lett 1962;8:250.
[4] Bean CP. Magnetization of high-field superconductors. Rev Mod Phys 1964;36:31.
[5] Barnes G, McCulloch M, Dew-Hughes D. Computer modeling of type II superconductors in applications. Supercond Sci Technol 1999;12:518.
[6] Amemiya N, Murasawa S, Banno N, Miyamoto K. Numerical modelings of superconducting wires for AC loss calculations. Physica C 1998;310:16–29.
[7] Brambilla R, Grilli F, Martini L. Development of an edge-element model for AC loss computation of high-temperature superconductors. Supercond Sci Technol 2007;20:16–24.
[8] Hong Z, Campbell AM, Coombs TA. Numerical solution of critical state in superconductivity by finite element software. Supercond Sci Technol 2006;19:1246.
[9] Grilli F, Brambilla R, Sirois F, Stenvall A, Memiaghe S. Development of a three-dimensional finite-element model for high-temperature superconductors based on the *H*-formulation. Cryogenics 2013;53:142–7.
[10] Farinon S, Fabbricatore P, Gomory F. Critical state and magnetization loss in multifilamentary superconducting wire solved through the commercial finite element code ANSYS. Supercond Sci Technol 2010;23:115004.
[11] Farinon S, Fabbricatore P, Grilli F, Krüger PAC. Applicability of the adaptive resistivity method to describe the critical state of complex superconducting systems. J Supercond Novel Magnetism 2012;25(7):2243–350.
[12] Chen G, Zhenghe H. Calculation of AC losses in HTS tape with FEA program ANSYS. IEEE Trans Appl Supercond 2005;15:2859.
[13] Prigozhin L. Analysis of critical-state problems in type-II superconductivity. IEEE Trans Appl Supercond 1997;7:3866–73.
[14] Sanchez A, Navau C. Magnetic properties of finite superconducting cylinders. I. Uniform applied field. Phys Rev B 2001;64:214506.
[15] Pardo E, Šouc J, Frolek L. Electromagnetic modelling of superconductors with a smooth current–voltage relation: variational principle and coils from a few turns to large magnets. Supercond Sci Technol 2015;2:044003.
[16] Grilli F, Pardo E, Stenvall A, Nguyen DN, Yuan W, Gomory F. Computation of losses in HTS under the action of varying magnetic fields and currents. IEEE Trans Appl Supercond 2014;24:8200433.
[17] Iannone G, De Marzi G, Farinon S, Fabbricatore P, Gambardella U. Modeling experimental magnetization cycles of thin superconducting strips by finite element simulations. IEEE Trans Appl Supercond 2015;25:8200107.
[18] Farinon S, Iannone G, Fabbricatore P, Gambardella U. 2D and 3D numerical modeling of experimental magnetization cycles in disks and spheres. Supercond Sci Technol 2014;27(10):104005.
[19] www.ansys.com; www.comsol.com.
[20] Fietz WA, Beasley MR, Silcox J, Webb WW. Magnetization of superconducting Nb-25%Zr wire. Phys Rev 1964;136:A335.
[21] Kim YB, Hempstead CF, Strnad AR. Critical persistent currents in hard superconductors. Phys Rev Lett 1962;9:306.
[22] Brandt EH. Superconductor disks and cylinders in an axial magnetic field. I. Flux penetration and magnetization curves. Phys Rev B 1998;58:6506.
[23] Chen DX, Goldfarb RB. Kim model for magnetization of type-II superconductors. J Appl Phys 1989;66:2489.
[24] Chen DX, Sanchez A, Muñoz JS. Exponential critical-state model for magnetization of hard superconductors. J Appl Phys 1990;67:3430.
[25] Johansen TH, Bratsberg H. Critical-state magnetization of type-II superconductors in rectangular slab and cylinder geometries. J Appl Phys 1995;77:8.
[26] Gömöry F, Tebano R, Sanchez A, Pardo E, Navau C, Husek I, et al. Current profiles and ac losses of a superconducting strip with an elliptic cross-section in a perpendicular magnetic field. Supercond Sci Technol 2002;15:1311–5.
[27] Bhagwat KV, Chaddah P. Magnetization curves of hard superconductor samples with non-zero demagnetization factor. J Phys 1989;33:4.
[28] Osborn JA. Demagnetizing factors of the general ellipsoid. Phys Rev 1945;67:351–7.
[29] Sanchez A, Navau C. Critical-current density from magnetization loops of finite high-Tc superconductors. Supercond Sci Technol 2001;14:444–7.
[30] Wilson MN. Superconducting magnets. Oxford: Clarendon Press; 1983.